Catalysis Today 158 (2010) 439–445

Contents lists available at ScienceDirect

Catalysis Today

journal homepage: www.elsevier.com/locate/cattod

# Characterization and performance of $V_2O_5$–$TiO_2$ catalysts prepared by rapid combustion method

Heqin Guo[a,b], Debao Li[a,*], Dong Jiang[a], Haicheng Xiao[a,b], Wenhuai Li[a], Yuhan Sun[a,*]

[a] State Key Laboratory of Coal Conversion, Institute of Coal Chemistry, Chinese Academy of Sciences, 27# Taoyuan South Road, Taiyuan, Shanxi 030001, PR China
[b] Graduate University of the Chinese Academy of Sciences, Beijing 100039, PR China

ARTICLE INFO

*Article history:*
Available online 13 July 2010

*Keywords:*
$VO_x$–$TiO_2$ catalysts
Rapid combustion method
Methanol oxidation reaction

ABSTRACT

The $VO_x$–$TiO_2$ (VT) catalysts were prepared by the rapid combustion (RC) method and characterized by SEM, XRD, Raman, XPS, $NH_3$-TPD and $H_2$-TPR techniques. The catalytic performance was evaluated in the methanol oxidation reaction. The SEM result showed that the VT catalysts were consisted of nanoparticle with mean grain size about 30 nm. The RC process enhanced the formation of $Ti_{(1-x)}V_xO_2$. The XRD and Raman results revealed that the vanadia transformed from the isolated $VO_x$ to polymeric $VO_x$ and then as crystalline $V_2O_5$ on the surface of $V_xTi_{(1-x)}O_2$. The polymeric $VO_x$ was predominant when $V_2O_5$ content was 30 wt.%. The $H_2$-TPR and $NH_3$-TPD results showed that the polymeric $VO_x$ exhibited more acidic sites and stronger reducibility than isolated $VO_x$ and crystalline $V_2O_5$. The catalytic activity result showed that the polymeric $VO_x$ was more active in methanol oxidation. The product distribution showed that the VT catalysts had redox-acidity bifunctional properties suitable for dimethoxymethane (DMM) synthesis, and the DMM selectivity was closely related to the reducibility and acidic sites.



## 1. Introduction

VT catalysts are widely used for many selective oxidation reactions. For example, they are used for ammoxidaion of alkyl aromatics [1,2], selective oxidation of methanol to formaldehyde (FA) [3] and methyl formate (MF) [4], selective oxidation of ethanol to acetaldehyde [5], selective oxidation of toluene to benzaldehyde and benzoic acid [6], selective oxidation of o-xylene to phthalic anhydride [7,8], etc.

It was well known that the structure, surface properties as well as catalytic performance of VT catalysts could be greatly influenced by the preparation method [9–11]. Several publications are available on the studies of these physico-chemical properties of VT catalyst prepared by coprecipitation, deposition and incipient wetness impregnation methods [12–15]. While, the study of these properties on VT catalyst prepared by the rapid combustion (RC) method has been rarely reported.

The RC method is a novel preparation method to produce the nanoscale catalysts, which typically involves a reaction in solution of metal nitrates and different fuels at high temperature [16–19]. These fuels reacting with oxygen-containing species, formed during the nitrates decomposition, provides rapid high-temperature interaction in the system. During this combustion reaction, various gas-phase products could be formed which inhibits particle size growth and increases specific surface area. Moreover, being the liquid state the initial reaction media (e.g., aqueous solution) allows mixing of the reactants on the molecular level, thus enhances the interaction between active species. And this might lead to the unique properties of the catalysts. Several publications are available on the preparation and characterization of iron-based, cobalt-based, cerium-based, etc., catalysts by RC method [16–21]. However, little attention has been paid to prepare the VT catalysts by this method. Therefore, the present work is focused on the study of the physico-chemical properties of VT catalysts prepared by RC method. In order to precisely characterize these properties, the methanol oxidation reaction is chosen as the probe reaction. That is because, in this reaction, the activity of the catalysts can reflect the existing state of vanadia [22–24], and the distribution of products can reflect the nature of the surface active sites: methanol is converted to formaldehyde (FA) and methyl formate (MF) on redox sites, to dimethyl ether (DME) on acidic sites and to dimethoxymethane on acidic and redox bifunctional sites (DMM) [21,25].

In the present work, the VT catalysts were prepared by RC method and the physico-chemical properties were characterized by SEM, BET, XRD, Raman, XPS, $H_2$-TPR and $NH_3$-TPD techniques. The catalytic performance was probed by the methanol oxidation in the presence of $O_2$. The purpose of this work is to determine the typical properties of VT (RC) catalysts.

* Corresponding authors. Tel.: +86 351 4068405.
*E-mail addresses:* dbli@sxicc.ac.cn (D. Li), yhsun@sxicc.ac.cn (Y. Sun).

0920-5861/$ – see front matter © 2010 Elsevier B.V. All rights reserved.
doi:10.1016/j.cattod.2010.06.007

**Table 1**
The textural properties, surface and bulk composition of the catalysts as well as the dispersion of vanadia.

| Sample | $S_{BET}$ ($m^2\ g^{-1}$) | Pore size (nm) | Pore volume ($cm^3/g$) | V/Ti[a] | V/Ti[b] | (V/Ti[a])/(V/Ti[b]) | V density calculated [c] ($1/nm^2$) | %w/w $TiO_2$ (cell volume A) | |
|---|---|---|---|---|---|---|---|---|---|
| | | | | | | | | Anatase | Rutile |
| $TiO_2$ (anatase) | 151.34 | 6.07 | 0.23 | – | – | – | – | 100 (137.62) | – |
| $TiO_2$ (rutile) | 34.54 | 6.20 | 0.05 | – | – | – | – | – | 100 (62.51) |
| 10VT | 29.29 | 10.42 | 0.08 | 0.34 | 0.078 | 4.35 | 18.6 | 31.2 (134.80) | 68.8 (61.76) |
| 20VT | 94.53 | 6.38 | 0.15 | 0.46 | 0.190 | 2.44 | 12.4 | 100 (134.70) | – |
| 25VT | 103.8 | 5.25 | 0.14 | 0.58 | 0.262 | 2.21 | 14.0 | 100 (135.20) | – |
| 30VT | 119.98 | 6.13 | 0.18 | 0.71 | 0.332 | 2.14 | 15.1 | 100 (134.51) | – |
| 40VT | 63.35 | 8.37 | 0.13 | 0.74 | 0.425 | 1.74 | 38.4 | 100 (135.80) | – |
| 50VT | 40.04 | 10.05 | 0.10 | 0.85 | 0.769 | 1.27 | 77.2 | 100 (135.20) | – |

[a] Surface atomic ratio calculated from XPS data.
[b] Bulk atomic ratio calculated from ICP-AES data.
[c] Supposing that all the vanadium atoms locate on the surface.

## 2. Experimental

### 2.1. Catalyst preparation

The VT catalysts were prepared by RC method. In the typical synthesis, 8.92 ml $TiCl_4$ was added to 24.26 ml 67 wt.% $HNO_3$ under vigorously stirring, and then 3.58 g $NH_4VO_3$ and 47.26 g carbamide were added to the solution. The obtained mixture was stirred until the $NH_4VO_3$ and carbamide were completely dissolved, and then calcined at 773 K for 10 min. According to $V_2O_5$ content in the final catalysts from ICP-AES (10, 20, 25, 30, 40 and 50 wt.%), the obtained catalysts were marked as 10VT, 20VT, 25VT, 30VT, 40VT and 50VT, respectively. For comparison, the pure anatase $TiO_2$ ($TiO_2$-A) and $V_2O_5$ were also prepared by RC method. And the rutile $TiO_2$ ($TiO_2$-R) was prepared by calcination of $TiO_2$-anatase at 873 K for 4 h.

### 2.2. Catalyst characterization

XRD patterns were measured on a Bruker Advanced X-Ray Solutions/D8-Advance scanning from 3° to 80° ($2\theta$) at a rate of 0.02°/s, using a Cu Kα radiation (λ = 0.15418 nm) source. The applied voltage and current were 50 kV and 35 mA, respectively. Raman spectra were measured using a Renishaw-UV–Vis Raman System 1000 Raman spectrometer (Kaiser Optical) and a frequency-doubled He:Cd laser at a wavelength of 325 nm. Raman spectra were measured using a Renishaw-UV–Vis Raman System 1000 Raman spectrometer. The excitation was provided by 514.5 nm line of an $Ar^+$ ion laser (Spectra Physics) employing a laser power of 7 mW. Surface areas of the catalysts were measured by a BET nitrogen adsorption method at 77.35 K using an ASAP 2000 machine. Prior to a measurement, the sample was degassed to $10^{-3}$ Torr at 473 K. The particle morphology (SEM) of the catalyst was observed by means of LEO 438VP scanning electron microscopy. The elemental analyses (Ti, V and S) were performed by inductively coupled plasma-optic emission spectroscopy (ICP-AES). The XPS measurements were performed in a Physical Electronics Company Quantum-2000 Scanning ESCA Microprobe equipped with an Al X-ray source (23.3 mA and 1.5 kV), a solid angle acceptance lens and a hemispherical electron analyzer. Samples were compressed in small cup under the pressure of 5 $kg/cm^2$ for 30 s and supported on a holding ceramic carousel. The positive charge, developed on the samples due to the photoejection process was compensated by a charge neutralizer (low energy electron and low energy ion beam). The residual pressure in the spectrometer chamber was $5 \times 10^{-7}$ Pa during data acquisition. The analyzed area of the sample was 100 μm and the energy region of the photoelectrons was scanned at a pass energy of 29.35 eV. The resolution was 0.68 eV. The binding energies were referenced to the C 1s band at 284.8 eV. The data were treated on Phi Multipack Program, Gaussian/Lorentzian = 80%. Atomic concentration ratios were calculated by correcting the measured intensity ratios with the manufacturer supplied sensitivity factor. The $H_2$-TPR measurements were carried out in continuous mode using a U-type quartz micro-reactor. A sample of about 25 mg was contacted with a $H_2$:$N_2$ mixture (5.13% volume of $H_2$ in $N_2$) at a total flow rate of 60 ml $min^{-1}$. The sample was heated at a rate of 10 K $min^{-1}$ from room temperature to 1173 K. The hydrogen consumption was monitored using a thermal conductivity detector (TCD). The $NH_3$-TPD spectra were recorded in a fixed-bed reactor system equipped with a gas chromatograph. The catalyst (200 mg) was pretreated at 773 K under Ar flow (60 ml $min^{-1}$) for 2 h and then cooled to 373 K under Ar flow. Then $NH_3$ was introduced into the flow system. The TPD spectra were recorded at a temperature rising rate of 10 K $min^{-1}$ from 373 to 900 K. The desorbed $NH_3$ was collected and titrated by 0.01 mol/l HCl. The amount of desorbed $NH_3$ was corresponding to the total number of acidic sites. According to the desorption temperature of $NH_3$, the acidity intensity could be determined. And based on the areas of desorption peaks, the number of acidic number for each type of acidity can be calculated.

## 3. Results and discussion

### 3.1. Physico-chemical characterization

The SEM photographs of the catalysts are shown in Fig. 1. The catalysts consisted of nanoparticle with an equable distribution except for a little aggregated particulate, and the morphology of the catalysts was homogeneous and had narrow distribution in grain size. The mean grain size was about 30 nm. The small particle size obtained on these catalysts might be due to the formation of gas-phase products during the high-temperature combustion reaction, which inhibited the growth of particle size.

The textural properties of the catalysts are shown in Table 1. The surface area of $TiO_2$-A was 151.34 $m^2\ g^{-1}$, while that for $TiO_2$-R was only 34.54 $m^2\ g^{-1}$, which might be due to the phase transformation of $TiO_2$-A to $TiO_2$-R at higher calcination temperature [25,26] (the $TiO_2$-R in the present study was prepared by calcination of $TiO_2$-A at 873 K for 4 h). For VT catalyst, with the increasing $V_2O_5$ content, the surface area of the obtained catalyst firstly increased then decreased, which reached the maximum on 30VT catalyst. The highest surface area obtained on 30VT catalyst might be responsible for the high dispersion of $VO_x$ on this catalyst (as discussed below).

The XRD patterns of the catalysts are shown in Fig. 2 and the typical diffraction peaks of $TiO_2$-A were observed for all the catalysts. For 10VT catalyst, the $TiO_2$-R phase was also observed, which disappeared with the increase of $V_2O_5$ content [27]. This indicated that the increase of $V_2O_5$ content inhibited the formation of $TiO_2$-

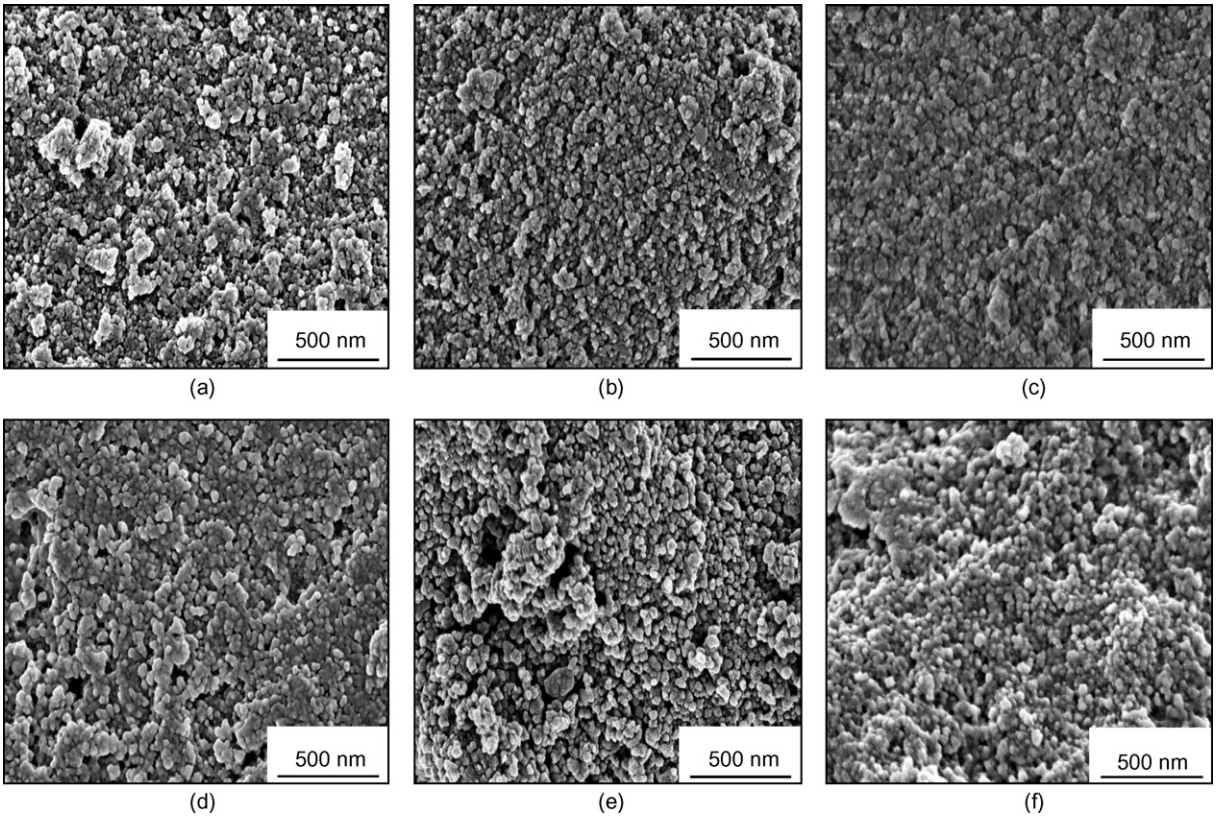


**Fig. 1.** The SEM photograph of the catalysts: 10VT (a), 20VT (b), 25VT (c), 30VT (d), 40VT (f) and 50VT (g).

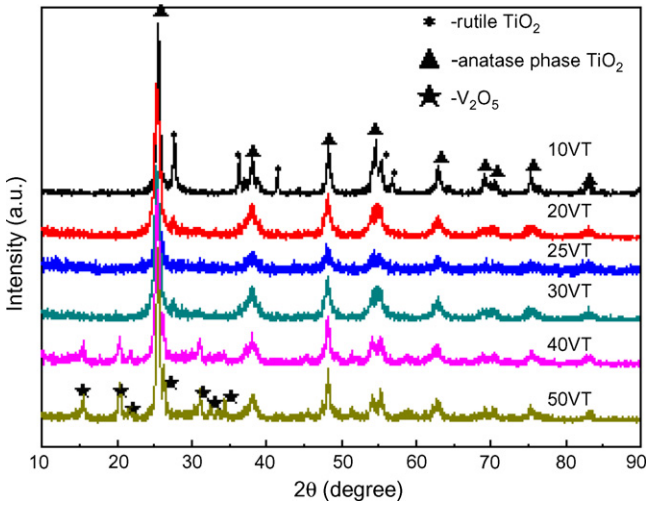


**Fig. 2.** The XRD patterns of the VT catalysts.

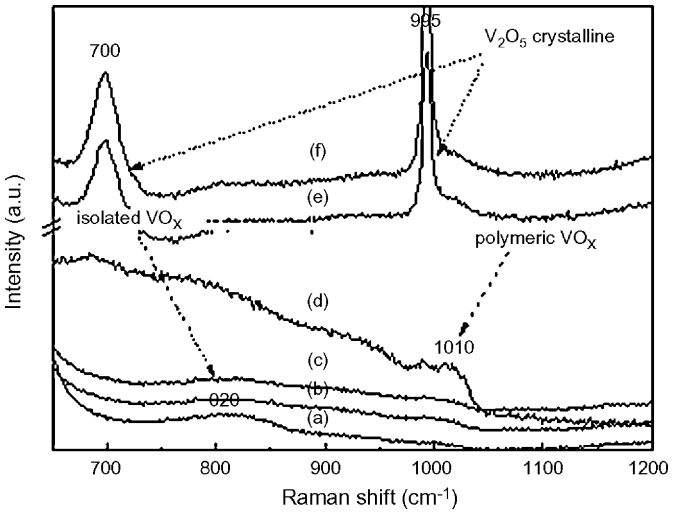


**Fig. 3.** The Raman spectra of the catalysts: 10VT (a), 20VT (b), 25VT (c), 30VT (d), 40VT (e) and 50VT (f).

R. For VT catalysts with $V_2O_5$ content below 30 wt.%, no crystalline $V_2O_5$ was observed, implying that the vanadia was highly dispersed or the $V_2O_5$ crystalline was less than 4 nm (beyond the detection capacity of the power XRD technique) [27]. The diffraction lines due to crystalline $V_2O_5$ began to appear when $V_2O_5$ content increased up to 40 wt.%, which suggested the agglomeration of $V_2O_5$ took place beyond this level of content.

To further study the existing state of vanadia, the Raman measurement was carried out (see Fig. 3). For 10VT catalyst, only a broad band around 820 $cm^{-1}$ assigned to the isolated $VO_4$ tetrahedral [28] was observed. As $V_2O_5$ content increased to 20 and 25 wt.%, a new band around 1010 $cm^{-1}$ due to the two-dimensional polymeric network of octahedral sharing corners and/or edges (polymeric $VO_x$) [26] appeared, simultaneously with the decrease of peak intensity at 820 $cm^{-1}$. For 30VT catalyst, the band intensity at 1010 $cm^{-1}$ was enhanced, implying the increased number of polymeric $VO_x$. Simultaneously, a weak band around 995 $cm^{-1}$ corresponding to the microcrystalline $V_2O_5$ was observed [15,27]. As $V_2O_5$ content increased to 40 and 50 wt.%, the band intensity of the typical $V_2O_5$ was enhanced with the disappearance of the band at 1010 $cm^{-1}$. Since the Raman response of the crystalline phases is intensive, the absence of crystalline $V_2O_5$ when $V_2O_5$ content was below 30 wt.% suggested that the vanadia was highly dispersed.

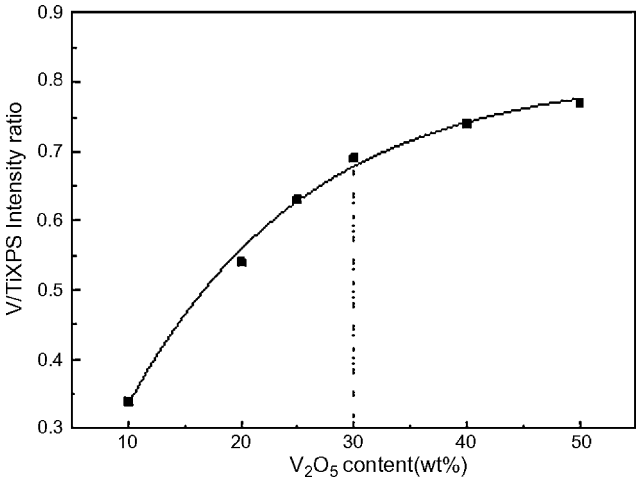


**Fig. 4.** XPS intensity ratio of $V2p_{3/2}$:$Ti2p_{3/2}$ as a function of $V_2O_5$ content in VT catalysts.

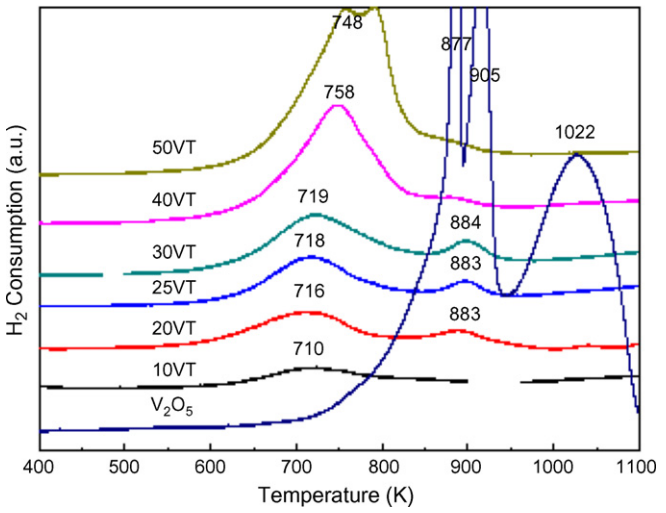


**Fig. 5.** The $H_2$-TPR profiles of the catalysts. A bulk $V_2O_5$ was also included for comparison.

In order to confirm the dispersion of vanadia, the surface and bulk composition of the catalysts were studied by XPS and ICP-AES techniques (see Table 1 and Fig. 4). It can be seen that the surface V:Ti ratio was higher than that of bulk, indicating that the vanadia mainly existed on the surface of the catalysts. Moreover, with the increase of $V_2O_5$ content, the $(V/Ti)_{surface}$:$(V/Ti)_{bulk}$ decreased, which implied the dispersion of vanadia decreased. This deduction can also be verified by the changes of XPS intensity ratio of $V2p_{3/2}$:$Ti2p_{3/2}$ (see Fig. 4). As $V_2O_5$ content increased, the XPS intensity ratio of $V2p_{3/2}$:$Ti2p_{3/2}$ increased up to 30 wt.% and did not change much at higher $V_2O_5$ content. Since the $V2p_{3/2}$:$Ti2p_{3/2}$ ratio indirectly provided the information about the dispersion of vanadia on titania, these results indicated that when $V_2O_5$ content was below 30 wt.%, the dispersion of vanadia was high, and as $V_2O_5$ content was above 30 wt.%, the dispersion decreased [23]. This result was in a good agreement with the Raman result. However, by calculating the numbers of V atom per $nm^2$ (Table 1), it was found that the numbers of V atom per $nm^2$ on 10VT, 20VT, 25VT and 30VT catalysts were about two times larger than that required to form the monolayer-dispersion (7–8 per $nm^2$ [29]). In other words, the crystalline $V_2O_5$ should be formed on these catalysts. However, the fact was not the case. It has been reported that the formation of solid solution $V_xTi_{(1-x)}O_2$ could lead to the absence of crystalline $V_2O_5$ even as $V_2O_5$ content was higher than that required to form monolayer-dispersion [12,25,26,30]. That was because the formation of $V_xTi_{(1-x)}O_2$ incorporated a large number of V into the solid solution. As a result, the surface number of V was few, not enough to form crystalline $V_2O_5$. Accordingly, in the present work, the cell volume of $TiO_2$ in the catalysts was calculated based on XRD data using the XRD-MDI Jade 5.0 software (see Table 1). As it can be seen, both the cell volumes of the $TiO_2$-A and $TiO_2$-R in the catalysts were smaller than those of pure $TiO_2$-A ($137.6 \pm 1.0$ Å$^3$) and $TiO_2$-R ($62.5 \pm 5 \times 10^{-2}$ Å$^3$), which suggested the formation of $Ti_{(1-x)}V_xO_2$ [25,26]. Therefore, it can be deduced that the high dispersion of vanadia when $V_2O_5$ content was below 30 wt.% should be due to the formation of $Ti_{(1-x)}V_xO_2$.

Based on the above analysis, the structure of VT catalysts can be deduced. As the $(V/Ti)_{surface}$ was higher than $(V/Ti)_{bulk}$, the vanadia should exist on the surface of the catalysts with $Ti_{(1-x)}V_xO_2$ as supports. As $V_2O_5$ content increased, the structure transformation of the catalysts can be depicted as Scheme 1. For 10VT catalyst, the unique Raman shift at 820 $cm^{-1}$ indicated that the vanadia mainly exited as isolated $VO_x$ (see Scheme 1(a)); for 20VT and 25VT catalysts, the appearance of Raman shift at 1010 $cm^{-1}$ and the decrease of the band intensity at 820 $cm^{-1}$ implied that the isolated and polymeric $VO_x$ coexisted on the surface (see Scheme 1(b)). As $V_2O_5$ content reached 30 wt.%, the increase of band intensity at 1010 $cm^{-1}$ and the appearance of a weak band around 995 $cm^{-1}$ suggested that the polymeric $VO_x$ was the predominant vanadia species, and the vanadia might monolayer dispersed (see Scheme 1(c)). As $V_2O_5$ content was higher than 40 wt.%, the enhanced band intensity at 700 and 995 $cm^{-1}$ indicated that the vanadia mainly existed as crystalline $V_2O_5$ (see Scheme 1(d)).

### 3.2. Redox and acidic properties

It is usually reported that the reducibility of vanadia-based catalysts is greatly influenced by the existing state of vanadia [27,30]. In order to study this effect, the TPR measurement was performed (see Fig. 5). The bulk $V_2O_5$ had three $H_2$ consumption peaks at 877 K, 905 K and 1022 K, respectively. Similar results were reported by Koranne et al. [31] and Bosch et al. [32], and they attributed this phenomenon to the following reduction sequence: $V_2O_5 \rightarrow V_6O_{13}$ (877 K), $V_6O_{13} \rightarrow V_2O_4$ (905 K), and $V_2O_4 \rightarrow V_2O_3$ (1022 K). After the addition of titania, the $H_2$ consumption peaks shifted to lower temperatures, which indicated that there was strong interaction between vanadia and titania [27,28]. As $V_2O_5$ content was below 30 wt.%, two $H_2$ consumption peaks at about 710 and 883 K were observed, and the peak intensity was enhanced with increasing $V_2O_5$ content, which indicated the increasing reducibility of the catalysts [32]. When $V_2O_5$ content reached 30 wt.%, the intensity of these reduction peak reached the maximum, which might be due to the largest number of polymeric $VO_x$ on this catalyst. As $V_2O_5$ content increased to 40 and 50 wt.%, the low reduction peak (710 K) shifted to higher temperature and the high reduction peak (883 K) shifted to lower temperature, and they finally appeared to merge into a single peak, which should be due to the reduction of crystalline $V_2O_5$ [31,33,34]. As $V_2O_5$ crystalline was difficult to reduce, the TPR results suggested that the reducibility of 10VT, 20VT, 25VT and 30VT catalysts was stronger than 40VT and 50VT catalysts. And the strongest $H_2$ consumption peaks at about 710 and 883 K observed on 30VT catalyst indicated the strongest reducibility of this catalyst.

The surface acidity of the catalysts was investigated by $NH_3$-TPD technique (see Table 2 and Fig. 6). There were two typical peaks for all the catalysts at 430–490 and 630–660 K, corresponding to the weaker acidic site (WAS) and middle stronger acidic site (MAS), respectively. For 10VT catalyst, the number of WAS was only 92.37 μmol $g^{-1}$. With the increase of $V_2O_5$ content, both the num-

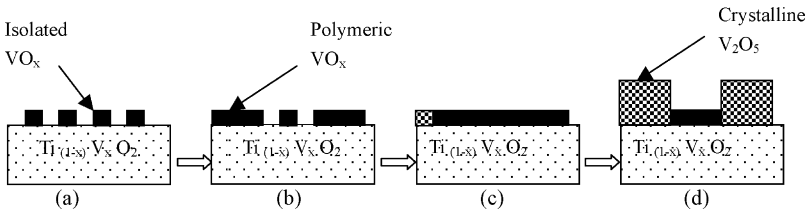


**Scheme 1.** A schematic of the transformation of vanadia on titania: (a) 10VT, (b) 20VT and 25VT, (c) 30VT, and (d) 40VT and 50VT.

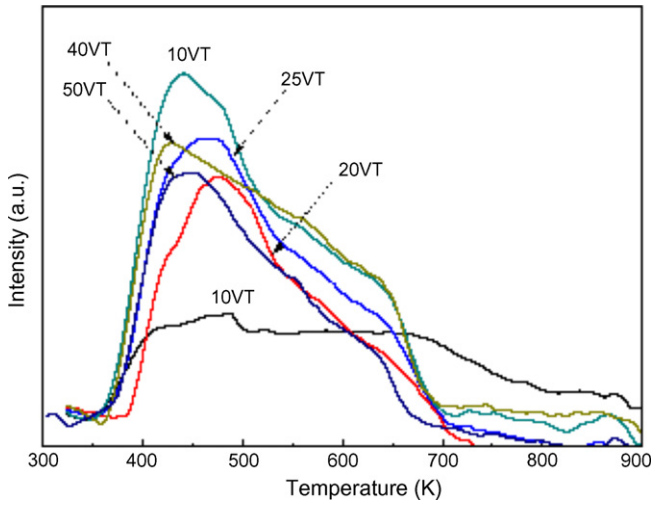


**Fig. 6.** The $NH_3$-TPD profiles of the catalysts.

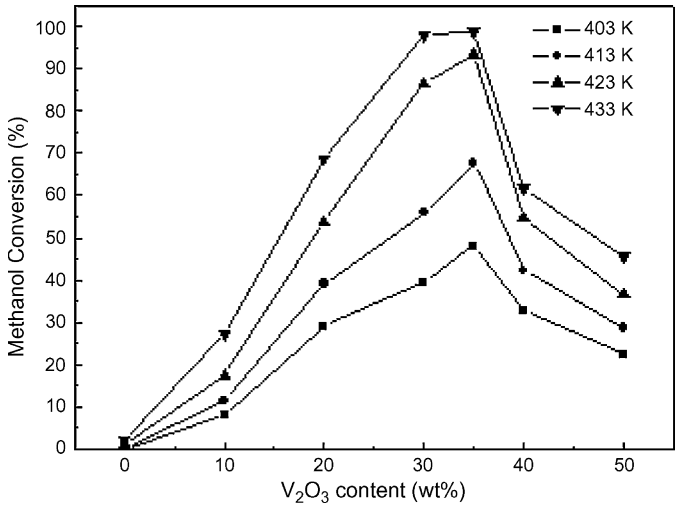


**Fig. 7.** The effect of $V_2O_5$ content on methanol conversion.

ber of WAS and MAS first increased and then decreased, which reached the maximum on 30VT catalyst, about 424.08 μmol $g^{-1}$ and 75.91 μmol $g^{-1}$, respectively. It was reported that the number of acidic sites of vanadium-based catalysts was related to the existing state of vanadia, and the high dispersion of vanadia contributed to larger number of acidic sites [35,36]. Combined with the Raman result, it can be deduced that the least number of acidic sites observed on 10VT catalyst could be due to the coverage of isolated $VO_x$. With the increase of $V_2O_5$ content, the appearance of polymeric $VO_x$ increased the acidic sites. As $V_2O_5$ content increased to 30 wt.%, the maximal population of acidic sites could be due to the largest number of polymeric $VO_x$. For catalysts with $V_2O_5$ content higher than 30 wt.%, the aggregation of $V_2O_5$ depleted some of the polymeric $VO_x$, which resulted in the declined number of acidic sites.

### 3.3. Catalytic performance

Fig. 7 shows the influence of $V_2O_5$ content on methanol conversion. As $V_2O_5$ content increased, the activity first increased and then decreased, which reached the maximum on 30VT catalyst. For example, at 433 K, the methanol conversion was only 27.12% on 10VT catalyst, while it increased up to 98.9% on 30VT catalyst and then decreased to 45.76% on 50VT catalyst. The performances at other reaction temperatures were similar to 433 K. The catalytic activity could be closely related to the existing state of vanadia. From the characterization results, it was known that the vanadia mainly existed as polymeric $VO_x$ on 30VT catalyst, as isolated or polymeric $VO_x$ when $V_2O_5$ content was below 30 wt.% and aggregated to crystalline $V_2O_5$ when $V_2O_5$ content was above 30 wt.%. Thus, it can be deduced that the polymeric $VO_x$ might be more active than the isolated $VO_x$ and crystalline $V_2O_5$.

In order to confirm this deduction, a plot between the TOF and $V_2O_5$ content (Fig. 8) was drawn, where TOF was equal to the num-

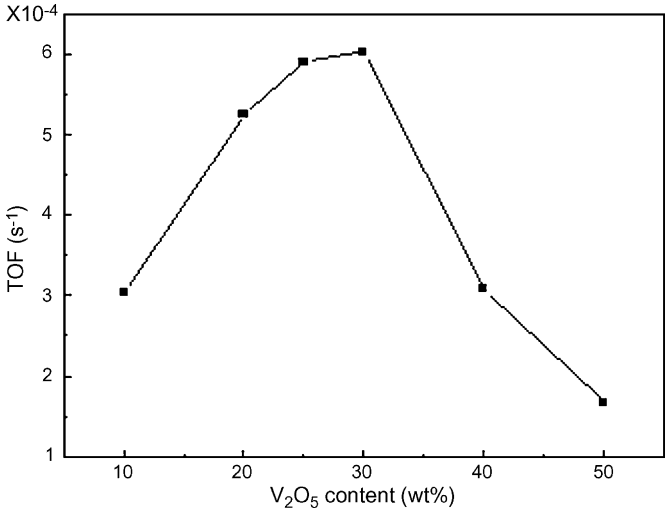


**Fig. 8.** The effect of $V_2O_5$ content on methanol turnover frequency.

**Table 2**
The $NH_3$-TPD results of the VT catalysts.

| Catalyst | Weak acidity | | Middle stronger acidity | |
|---|---|---|---|---|
| | T (K) | Number (μmol $g^{-1}$) | T (K) | Number (μmol $g^{-1}$) |
| $TiO_2$ | 480 | 205.00 | 660 | 169.20 |
| 10VT | 475 | 92.37 | – | – |
| 20VT | 473 | 338.31 | 640 | 24.56 |
| 25VT | 460 | 381.20 | 638 | 50.23 |
| 30VT | 430 | 424.08 | 635 | 75.91 |
| 40VT | 425 | 259.80 | 635 | 45.52 |
| 50VT | 425 | 260.50 | 635 | 41.99 |

**Table 3**
The effect of $V_2O_5$ content on DMM selectivity.

| Catalysts | Selectivity (%) | | | | |
|---|---|---|---|---|---|
| | FA | DME | MF | DMM | $CO_x$ |
| 10VT | 14.82 | 0.12 | 14.47 | 69.90 | 0.70 |
| 20VT | 3.47 | 0.00 | 13.66 | 82.64 | 0.23 |
| 25VT | 3.95 | 0.00 | 8.23 | 86.47 | 0.35 |
| 30VT | 2.98 | 0.57 | 6.63 | 89.76 | 0.06 |
| 40VT | 4.93 | 0.00 | 9.02 | 85.50 | 0.55 |
| 50VT | 12.25 | 0.57 | 12.16 | 74.54 | 0.48 |

$Ar/O_2/CH_3OH = 84.6/9.4/6.0$, 393 K at about 33% methanol conversions.

ber of methanol converted per second per vanadia species. As it can be seen, with the increase of $V_2O_5$ content, the TOF showed similar trend to the activity, which was in line with the changing trend of the number of polymeric $VO_x$. This result indicated that the polymeric $VO_x$ was more active in methanol oxidation, and this deduction was consisted with the previous reports of Elmi [22] and Chary et al. [23]. According to their study, the active sites in methanol oxidation were vanadium ions on the surface and the optimal activity were given by a site having both vanadium and X (represent the support) as neighbors (V–O–V*–O–X). When $V_2O_5$ content was below monolayer level, the X–O–V*–O–X (isolated $VO_x$) was predominant; at monolayer loading level, the X–O–V*–O–V (polymeric $VO_x$) was present; higher than monolayer loading, the V–O–V*–O–V ($V_2O_5$ crystalline) was formed. Both X–O–V*–O–X and V–O–V*–O–V were not very active. Combined with the characterization result, it was reasonable to deduce that on 10VT catalyst, the vanadia mainly exited as isolated $VO_x$ bounded to titania surface through the Ti–O–V*–O–Ti, leading to low TOF. With the increase of $V_2O_5$ content, some of Ti–O–V*–O–Ti was replaced by Ti–O–V*–O–V, which led to the increase of TOF. The highest TOF observed on 30VT catalyst might be due to the presence of both vanadium and titanium as neighbors (predominant existed as Ti–O–V*–O–V). As $V_2O_5$ content was above 30 wt.%, the number of Ti–O–V*–O–V decreased, simultaneously with the increasing number of V–O–V*–O–V, which resulted in the decrease of TOF. From above analysis, it can be concluded that the polymeric $VO_x$ was more active than the isolated $VO_x$ and the crystalline $V_2O_5$ in methanol oxidation.

Table 3 shows the product distribution over VT catalyst at similar methanol conversion (about 33%). The VT catalysts exhibited a high selectivity to DMM with low or none selectivity to FA, MF and DME. As FA and MF are produced on redox sites, DME on acidic sites, and DMM on redox–acidic bifunctional sites [21,25]. This product distribution indicated the VT catalysts exhibited redox–acidic bifunctional properties suitable for DMM synthesis. Thus, the changes of DMM selectivity can reflect the redox and acidity properties of the catalyst. As $V_2O_5$ content increased, DMM selectivity first increased and reached the maximum on 30VT catalyst (89.76%), and then decreased. According to the mechanism of the one-step synthesis of DMM from methanol reported by Liu and Iglesia [37], methanol was primarily oxidized to FA on the redox sites, and then methanol reacted with FA to form DMM on acidic sites. Combined with the $H_2$-TPR and $NH_3$-TPD results, it seemed that the highest DMM selectivity obtained on 30VT catalyst could be due to its stronger reducibility to catalyze the first reaction and its high corresponding population of acidic sites to catalyze the second reaction. For 20VT and 25VT catalysts, although the reducibility was strong enough to catalyze the first reaction, the small number of acidic sites was not enough to catalyze the second reaction, which led to lower DMM selectivity. And this deduction can also be verified by the higher selectivity of FA and MF on these catalysts. For 10VT, 40VT and 50VT catalysts, the poor reducibility of isolated $VO_x$ and crystalline $V_2O_5$ did not have enough reducibility to catalyze the first reaction and the small number of acidic sites could not efficiently catalyze the second reaction, leading to low DMM selectivity.

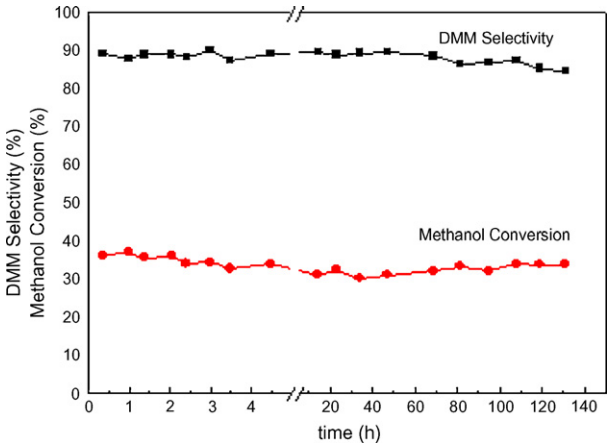


**Fig. 9.** The changes of methanol conversion and DMM selectivity with time on stream (30VT).

The stability test was carried for 30VT catalyst at 393 K (see Fig. 9). The result showed that DMM selectivity and methanol conversion did not change much with the increase of the time on stream, which indicated that the VT catalysts had a better stability.

## 4. Conclusion

VT catalysts prepared by RC method were consisted of nanoparticle with mean grain size of about 30 nm. The RC process enhanced the formation of $Ti_{(1-x)}V_xO_2$, which acted as supports with $VO_x$ covered on its surface. As $V_2O_5$ content increased, the vanadia transformed from the isolated $VO_x$ to polymeric $VO_x$ and then as crystalline $V_2O_5$. The polymeric $VO_x$ was predominant on 30VT catalyst. Moreover, The 30VT catalyst showed the best catalytic performance (with 89.76% DMM selectivity for 33% methanol conversion), which should be attributed to its strongest reducibility and largest number of acidic sites. Consequently, the structure, acidity and redox properties of the catalysts were related with the $V_2O_5$ content, which finally affected the catalytic behavior of in the methanol oxidation reaction.

## Acknowledgments

This work was supported by the Key Project of Natural Science Foundation of China (No. 20603045) and the International Sci. & Tech. Cooperation Project of Ministry of Science and Technology of China (No. 2007DFC60110).

## References

[1] P. Cavalli, F. Cavani, I. Manenti, F. Trifiro, Catal. Today 1 (1987) 245.
[2] M. Sanati, A. Andersson, J. Mol. Catal. 59 (1990) 233.
[3] F. Roozeboom, P.D. Cordingley, P.J. Gellings, J. Catal. 68 (1981) 464.
[4] P. Forzatti, E. Tronconi, G. Busca, P. Tittarelli, Catal. Today 1 (1987) 209.
[5] N.E. Quaranta, J. Soria, V.C. Corberan, J.L.G. Fierro, J. Catal. 171 (1997) 1.
[6] D.A. Bulushev, L. Kiwi-Minsker, V.I. Zaikovskii, A. Renken, J. Catal. 193 (2000) 145.
[7] M. Wainwright, N. Foster, Catal. Rev. Sci. Eng. 19 (1979) 211.
[8] V. Nikolov, D. Klissurski, A. Anastasov, Catal. Rev. Sci. Eng. 33 (1991) 319.
[9] F. Roozeboom, T. Fransen, P. Mars, P.J. Gellings, Z. Anorg, Allg. Chem. 449 (1979) 25.
[10] G. Hausinger, H. Schmelz, H. Knijzinger, Appl. Catal. 39 (1988) 267.
[11] M.P. Casaletto, L. Lisi, G. Mattogno, P. Patrono, F. Pinzari, G. Ruoppolo, Catal. Today 91–92 (2004) 271.
[12] L.E. Briand, R.D. Bonetto, M.A. Sanchez, H.J. Thomas, Catal. Today 32 (1996) 205.
[13] J. Androulakis, N. Katsarakis, J. Giapintzakis, N. Vouroutzis, E. Pavlidou, K. Chrissafis, E.K. Polychroniadis, V. Perdikatsis, J. Solid State Chem. 173 (2003) 350.

[14] L.A. Isupova, G.M. Alikina, S.V. Tsybulya, A.N. Salano, N.N. Boldyreva, E.S. Rusina, I.A. Ovsyannikova, V.A. Rogov, R.V. Bunina, V.A. Sadykov, Catal. Today 75 (2002) 305.
[15] J.W. Liu, Y.C. Fu, Q. Sun, J.Y. Shen, Micropor. Mesopor. Mater. 116 (2008) 614.
[16] P. Bera, K.C. Patil, V. Jayaram, G.N. Subbanna, M.S. Hegde, J. Catal. 196 (2000) 293.
[17] M. Alifanti, N. Blangenois, M. Florea, B. Delmon, Appl. Catal. A: Gen. 280 (2005) 255.
[18] P. Bera, K.R. Priolkar, A. Gayen, P.R. Sarode, M.S. Hegde, S. Emura, R. Kumashiro, V. Jayaram, G.N. Subbanna, Chem. Mater. 15 (2003) 2049.
[19] S.L. Gonzalez-Cortes, T.C. Xiao, P.M.F.J. Costa, B. Fontal, M.L.H. Green, Appl. Catal. A: Gen. 270 (2004) 209.
[20] K.R. Priolkar, P. Bera, P.R. Sarode, M.S. Hegde, S. Emura, R. Kumashiro, N.P. Lalla, Chem. Mater. 14 (2002) 2120.
[21] J.M. Tatibouet, Appl. Catal. A 148 (1997) 213.
[22] A.S. Elmi, T. Enrico, C. Cinzia, J.P. Gomez Martin, P. Forzatti, Ind. Eng. Chem. Res. 28 (1989) 387.
[23] K.V.R. Chary, G. Kishan, C.P. Kumar, U.V. Sagar, J.W. Niemantsverdriet, Appl. Catal. A: Gen. 245 (2003) 303.
[24] M. Badlani, I.E. Wachs, Catal. Lett. 75 (2001) 137.
[25] R.Y. Saleh, I.E. Wachs, S.S. Chan, C.C. Chersich, J. Catal. 98 (1986) 102.
[26] M.A. Banares, L.J. Alemany, M.C. Jimeńez, M.A. Larrubia, F. Delgado, M.L. Granados, A.M. Arias, J.M. Blasco, J.G. Fierro, J. Solid State Chem. 124 (1996) 69.
[27] Q. Sun, Y.C. Fu, J.W. Liu, A. Auroux, J.Y. Shen, Appl. Catal. A: Gen. 334 (2008) 26.
[28] F. Roozeboom, M.C. Mittelmeijer-Hazeleger, J.A. Moulljn, J. Medema, V.H.J. Beer, P.J. Gellngs, J. Phys. Chem. 84 (1980) 2783.
[29] I.E. Wachs, B.M. Weckhuysen, Appl. Catal. A 157 (1997) 67.
[30] L. Briand, L. Gambaro, H. Thomas, J. Catal. 161 (1996) 839.
[31] M.M. Koranne, J.G. Goodwin Jr., G. Marcelin, J. Catal. 148 (1994) 369.
[32] H. Bosch, B.J. Kip, J.G. Van Ommen, P.J. Gellings, J. Chem. Soc., Faraday Trans. 80 (1984) 2479.
[33] L. Nalbandian, A.A. Lemonidou, Thermochim. Acta 419 (2004) 149.
[34] H. Poelman, B.F. Sels, M. Olea, K. Eufinger, J.S. Paul, B. Moens, I. Sack, V. Balcaen, F. Bertinchamps, E.M. Gaigneaux, P.A. Jacobs, G.B. Marin, D. Poelman, R. De Gryse, J. Catal. 245 (2007) 156.
[35] M. Kobayashi, M. Hagi, Appl. Catal. B: Environ. 63 (2006) 104.
[36] M. Niwa, Y. Habuta, K. Okumura, N. Katada, Catal. Today 87 (2003) 213.
[37] H.C. Liu, E.S. Iglesia, J. Phys. Chem. B 109 (2005) 2155.